Stochastics and Dynamics, Vol. 4, No. 2 (2004) 185–200

World Scientific
www.worldscientific.com

QUANTUM AND THERMAL CORRECTIONS TO A CLASSICALLY CHAOTIC DISSIPATIVE SYSTEM

MANUEL RODRÍGUEZ-ACHACH* and GABRIEL PÉREZ

Departamento de Física Aplicada, Cinvestav del IPN, Unidad Mérida, A. P. 73 "Cordemex", 97310 Mérida, Yucatán, México
**achach@gema.mda.cinvestav.mx*

HILDA A. CERDEIRA

International Centre for Theoretical Physics Trieste, Italy

Received 22 September 2003
Revised 1 April 2004

The effects of quantum and thermal corrections on the dynamics of a damped nonlinearly kicked harmonic oscillator are studied. This is done via the quantum Langevin equation formalism working on a truncated moment expansion of the density matrix of the system. We find that the type of bifurcations present in the system change upon quantization and that chaotic behavior appears for values of the nonlinear parameter that are far below the chaotic threshold for the classical model. Upon increase of temperature or Planck's constant, bifurcation points and chaotic thresholds are shifted towards lower values of the nonlinear parameter. There is also an anomalous reverse behavior for low values of the cutoff frequency.

Keywords: Quantum chaos; dissipative systems; Langevin equation.

PACS Nos.: 05.45.+b, 03.65.Sq, 05.40.+j, 42.50.Lc

1. Introduction

With the impressive results obtained in the theory of classical chaos, the interest in the manifestations of chaos in quantum systems has grown over the past years. Although the difference between chaotic and regular dynamics for quantized Hamiltonian dynamics is not very significant, some insight has been gained with the quantization of conservative models with chaotic classical counterparts. Among the peculiar phenomenology that has been found we have the appearance of *scars*, which are wave functions with enhanced amplitude along the paths of classical unstable periodic orbits [1–4]. Further connection between classically unstable orbits and quantum behavior has been given by Gutzwiller's trace formula for the density of states [5,6], which has been applied with some success to many hyperbolic systems [7]. A connection has also been found between the nature of the classical dynamics, be it regular or chaotic, and the statistics of the energy spectrum, which obeys the general distributions found in random matrix theory [8, 9].

However, for systems that include dissipation, not much work has been done. This is an important subject of study because, besides its theoretical interest, it is of central importance in several interesting applications (SQUIDS, tunneling phenomena, etc.). The main problem with such systems is the presence of the dissipative term, which makes the quantization process not feasible by standard methods. Approaches to this problem have been proposed by many authors over the last three decades. Kostin proposes the use of a nonlinear Schrödinger equation for the process of quantization [10], but it has some problems with the superposition principle and yields results of an unphysical nature. Dekker [11] uses a canonical quantization method based on complex variables, with some degree of success, but the physical basis of his theory is not very clear. Maximal entropy methods [12] have also been proposed, using a coupling between quantum and classical degrees of freedom. This approach ignores the effects of thermally driven fluctuations.

In general, the only fully successful and physically sound quantization scheme for dissipative systems is the so-called system-plus-reservoir approach, in which one considers the system coupled to a large reservoir or heath bath. Since the entire system plus reservoir may be considered as closed, one can apply to it the standard rules of quantization, paying of course the penalty of dealing with an infinite number of degrees of freedom. Dissipation comes about by the net transfer of energy from the system to the reservoir, and thermal fluctuations appear as a result of the random energy exchange from/to the heat bath. These approaches ensure the non-violation of commutator rules, and include the appropriate fluctuation-dissipation relations.

Some common approaches using the system-plus-reservoir picture are the influence-functional methods introduced by Feynman and Vernon [13], that have been used by Caldeira and Legget to study quantum Brownian motion [14] and dissipative tunneling effects [15]; generalized master equations [16], used to describe damping phenomena in quantum optics and spin dynamics [17, 18]; and quantum Langevin equations [19], used by Ford *et al.* to study dissipative quantum tunneling at zero temperature [20].

In the area of nonlinear (and classically chaotic) dissipative models, there are some results that point to the conclusion that quantum effects act as sources of noise. As a result, it is expected that the threshold for chaos be lowered *in a continuous fashion* upon the introduction of quantum corrections. This was reported by Graham and Tel [21], who worked in the master equation formalism [18, 22] to quantize Henon's map, and by Cerdeira *et al.* [23], who built a quantum mapping of Wigner functions for a kicked oscillator. More recently, Cohen [24] studied the quantum dissipative kicked rotator using influence functionals, while Dittrich and Graham used the master equation formalism for the same purpose [25]. Liu and Schieve [26] use the quantum Langevin equation approach to show that a chaotic attractor is observed in a quantum system whose classical counterpart is non-chaotic. In contradiction to these works, there were some results showing an

increase of order (a raising of the chaoticity thresholds) for a kicked dissipative oscillator [27].

In this work we study the behavior of a periodically kicked harmonic oscillator, with dissipation, and in the presence of quantum and thermal fluctuations. Our interest is mostly to find how the bifurcation points and chaotic thresholds in parameter space change when increasingly large thermal and quantum effects are included. To do this, we generate a mapping of expectation values, using a quantum Langevin approach, that has an immediate analog with its classical limit. This expectation values mapping (EVM) constitutes in principle a complete description of the quantum dynamics, based in a discrete set of variables, and has the advantage of exhibiting a clear hierarchy in its terms, introducing from the beginning mean values and a sequence of moments of the fluctuations.[a] It should be noted, however, that the sequence of bifurcations and the property of a map to be chaotic, is a mathematical property which depends on the model and the approximations used.

In Sec. 2 we introduce the classical model, a harmonic oscillator with a periodic "kick" from a nonlinear potential. In Sec. 3 we will use the Langevin equation formalism to obtain a quantal version of the classical map of the preceding section. The resulting (truncated) EVM will include both thermal and quantum corrections; the change in the behavior of the dynamics as function of $k_{\mathrm{B}}T$ and $\hbar$ is examined. In Secs. 4 and 5 we show and discuss the results obtained and give some concluding remarks.

2. Classical Kicked Harmonic Oscillator with Damping

Starting with the Hamiltonian for a kicked oscillator

$$H = \frac{p^2}{2m} + \frac{1}{2}m\Omega^2 x^2 + V(x)\sum_n \delta(t - n\tau), \tag{2.1}$$

where τ is the period of the kick, we introduce the dissipative force $2\gamma\dot{x}$ to obtain the equations of motion in the form

$$\dot{p} = -m\Omega^2 x - 2\gamma\frac{p}{m} - V'(x)\sum_n \delta(t - n\tau), \tag{2.2}$$

$$\dot{x} = \frac{p}{m}. \tag{2.3}$$

From now on we will set the units of mass and time so that $m = 1$ and $\Omega = 1$. For times $t \neq n\tau$, the kick has no effect so we get the equation

$$\ddot{x} + 2\gamma\dot{x} + x = 0, \tag{2.4}$$

whose well-known underdamped ($\gamma < 1$) solution is given by

$$x(t) = e^{-\gamma t}(A\cos\omega_0 t + B\sin\omega_0 t), \tag{2.5}$$

$$p(t) = e^{-\gamma t}\left[\omega_0(-A\sin\omega_0 t + B\cos\omega_0 t) - \gamma(A\cos\omega_0 t + B\sin\omega_0 t)\right], \tag{2.6}$$

[a]The completeness of the description given by the EVM is shown in appendix A in quant-ph/0404001.

where $\omega_0 = \sqrt{1-\gamma^2}$, and A and B are given in terms of initial conditions. Evaluating these constants, and defining an evolution matrix T by

$$T_{QQ} \equiv \exp(-\gamma\tau)(\cos(\omega_0\tau) + \gamma\sin(\omega_0\tau)/\omega_0), \tag{2.7}$$

$$T_{QP} \equiv \exp(-\gamma\tau)\sin(\omega_0\tau)/\omega_0, \tag{2.8}$$

$$T_{PQ} \equiv -\exp(-\gamma\tau)(\omega_0 + \gamma^2/\omega_0)\sin(\omega_0\tau), \tag{2.9}$$

$$T_{PP} \equiv \exp(-\gamma\tau)(\cos(\omega_0\tau) - \gamma\sin(\omega_0\tau)/\omega_0), \tag{2.10}$$

we can write a discrete linear map corresponding to Eqs. (2.5) and (2.6)

$$x^-_{n+1} = T_{QQ}\, x^+_n + T_{QP}\, p^+_n, \tag{2.11}$$

$$p^-_{n+1} = T_{PQ}\, x^+_n + T_{PP}\, p^+_n, \tag{2.12}$$

where we have set as usual $x^-_n \equiv x(n\tau - 0^+)$, $x^+_n \equiv x(n\tau + 0^+)$, with similar definitions for p. We need now to calculate how the kick affects the dynamics, in order to complete the map. This can be done by integrating Eq. (2.2) from just before to just after $t = (n+1)\tau$. Over this region x is continuous and thus we obtain

$$p^+_{n+1} - p^-_{n+1} = -V'(x^-_{n+1}), \tag{2.13}$$

$$x^+_{n+1} = x^-_{n+1}. \tag{2.14}$$

Successive application of the mappings (2.5), (2.6) and (2.13), (2.14) will give us a map that yields the values for x and p just after each kick (discard the superscripts from now on):

$$x_{n+1} = T_{QQ}\, x_n + T_{QP}\, p_n, \tag{2.15}$$

$$p_{n+1} = T_{PQ}\, x_n + T_{PP}\, p_n - V'(x_{n+1}). \tag{2.16}$$

We have chosen the force acting on the kicks as

$$V'(x) = -V_0 e^{-(x/a)^2}, \tag{2.17}$$

which gives a potential bounded from below. From now on we will set the units of length so that $a = 1$. This force is maximum at $x = 0$, so that the closer the harmonic oscillator gets to its rest position, the stronger the repulsive effect of the kick becomes. We are interested in a region of parameter space such that $\gamma \ll \omega$, and where clear chaotic behavior can be found. After some search, we have chosen $\gamma = 0.03$ and $\tau = 10.0$. For bifurcation diagrams given in terms of V_0, we find a well-defined transition to chaos around $V_0 \approx 5.69287$. It should be noticed that there is some coexistence of attractors in this sector of parameter space; these attractors evolve from order to chaos following Feigenbaum scenario (see Fig. 1). For the fully chaotic region, the attractors are Hénon-like (see Fig. 2).

The later map will be quantized in the next section in order to see the temperature and quantum effects on the dynamics.

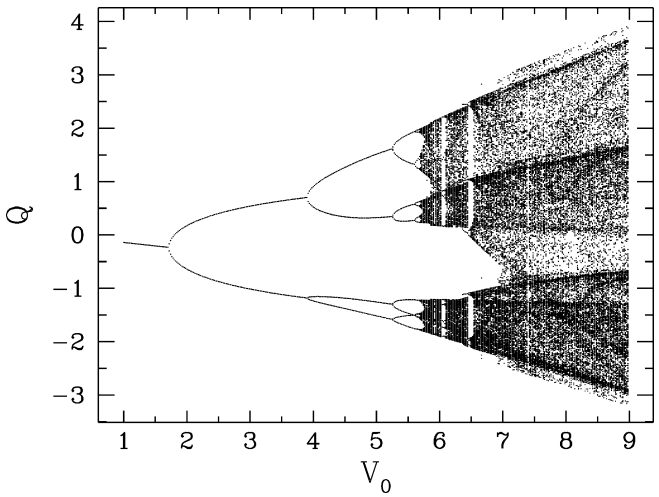

Fig. 1. Bifurcation diagram for the classical system for $1 < V_0 < 9$. Here we have set $\gamma = 0.03$, $\tau = 10$ and use 100 random initial conditions for each value of V_0.

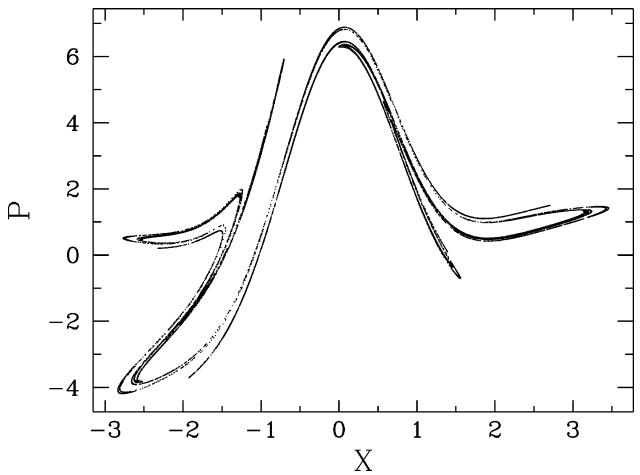

Fig. 2. Attractor for the classical system using the same parameters as in Fig. 1, and a value of $V_0 = 8.0$.

3. Quantization of the Kicked Harmonic Oscillator with Damping

We use the Langevin equation formalism for the process of quantization. This equation is obtained from the quantization in the Heisenberg picture of a closed system given by a relevant degree of freedom $\mathbf{Q}$, in contact with a large (in the limit, infinite) bath of harmonic oscillators $\mathbf{q}_j$. It is given by

$$\ddot{\mathbf{Q}} + 2\int_{t_e}^{t} \Gamma(t-t')\dot{\mathbf{Q}}dt' + W'(\mathbf{Q}) = \mathbf{F}(t), \tag{3.1}$$

where $\mathbf{Q}(t)$ and $\mathbf{F}(t)$ are operators, $W(\mathbf{Q})$ is the potential and $\mathbf{F}(t)$ is a random force that, together with the memory function $\Gamma(t)$, depends on the characteristics of the bath. These oscillators are assumed to be in thermal equilibrium at some initial time t_e. The memory function $\Gamma(t)$, and the expectation value and symmetric correlations of $\mathbf{F}(t)$ are given by [19]

$$\langle \mathbf{F}(t) \rangle = 0, \tag{3.2}$$

$$\langle \mathbf{F}(t)\mathbf{F}(t') + \mathbf{F}(t')\mathbf{F}(t) \rangle = \sum_j \hbar m_j \omega_j^3 \coth\left(\frac{\hbar\omega_j}{2k_{\mathrm{B}}T}\right) \cos[\omega_j(t-t')], \tag{3.3}$$

$$\Gamma(t) = \frac{1}{2}\sum_j m_j \omega_j^2 \cos(\omega_j t)\Theta(t), \tag{3.4}$$

where m_j and ω_j are the mass and frequency of the jth oscillator. These expressions imply a quantum fluctuation-dissipation theorem. It is assumed that no correlation exists between $\mathbf{F}$ and $\mathbf{Q}$ or $\mathbf{P}$. This implies ignoring some switch-on processes, which arise due to our assumption that the bath *per se* is in thermal equilibrium at time t_e.

From now on, we will use a bath of equal masses and a white (i.e. ω-independent), and continuous frequency distribution, which is the case for constant friction or Markovian approximation. In this case,

$$\Gamma(t) = 2\gamma\delta(t), \tag{3.5}$$

$$\langle \mathbf{F}(t)\mathbf{F}(t') + \mathbf{F}(t')\mathbf{F}(t) \rangle = \frac{2\gamma}{\pi}\int_o^\infty d\omega\, \hbar\omega \coth\left(\frac{\hbar\omega}{2k_{\mathrm{B}}T}\right) \cos[\omega(t-t')], \tag{3.6}$$

and Eq. (3.1) reduces to the simpler form

$$\ddot{\mathbf{Q}} + 2\gamma\dot{\mathbf{Q}} + W'(\mathbf{Q}) = \mathbf{F}(t). \tag{3.7}$$

The drawback of using the Markovian approximation is that it will generate some divergences since we now have contributions from arbitrarily high frequencies in the bath. We will use the same harmonic oscillator-plus-kick potential indicated in the Hamiltonian (2.1) and Eq. (2.17). Between kicks, the (underdamped) solution of Eq. (3.7) is given by

$$\mathbf{Q}(t) = e^{-\gamma t}(\mathbf{A}\cos\omega_0 t + \mathbf{B}\sin\omega_0 t) + \mathbf{f}(t,\omega_0,\gamma), \tag{3.8}$$

$$\mathbf{P}(t) = \dot{\mathbf{Q}}(t), \tag{3.9}$$

where the solution for nonhomogeneous part has been obtained from a Riccatti equation and we have defined ω_0 in an analogous way as for the classical case. The operators $\mathbf{A}$ and $\mathbf{B}$ are given in terms of initial conditions, evaluated at some initial time t_0 (not to be confused with t_e), and the inhomogeneous term is

$$\mathbf{f}(t,\omega_0,\gamma) = \frac{1}{\omega_0}\int_{t_0}^t dt' e^{-\gamma(t-t')}\sin\omega_0(t-t')\mathbf{F}(t'). \tag{3.10}$$

For the moment $\mathbf{P}$ we get

$$\begin{aligned}\mathbf{P}(t) = &-\gamma e^{-\gamma t}\left[\mathbf{A}\cos(\omega_0 t) + \mathbf{B}\sin(\omega_0 t)\right] \\ &+ \omega_0 e^{-\gamma t}\left[-\mathbf{A}\sin(\omega_0 t) + \mathbf{B}\cos(\omega_0 t)\right] + \mathbf{g}(t,\omega_0,\gamma),\end{aligned} \tag{3.11}$$

where

$$\mathbf{g}(t,\omega_0,\gamma) = \frac{1}{\omega_0}\int_{t_0}^{t} dt' e^{-\gamma(t-t')}\left[-\gamma\sin\omega_0(t-t') + \omega_0\cos\omega_0(t-t')\right]\mathbf{F}(t'). \quad (3.12)$$

Now we will take the integration limits to be $t_0 \to n\tau^+$ and $t \to (n+1)\tau^-$, so we can evaluate the initial conditions and obtain

$$\mathbf{Q}^-_{n+1} = T_{QQ}\,\mathbf{Q}^+_n + T_{QP}\,\mathbf{P}^+_n + \mathbf{f}(\tau,\omega_0,\gamma), \quad (3.13)$$

$$\mathbf{P}^-_{n+1} = T_{PQ}\,\mathbf{Q}^+_n + T_{PP}\,\mathbf{P}^+_n + \mathbf{g}(\tau,\omega_0,\gamma), \quad (3.14)$$

with the same matrix elements T_{ij} defined before. Defining the fluctuations as

$$\delta\mathbf{X} \equiv \mathbf{X} - \langle\mathbf{X}\rangle, \quad (3.15)$$

we can now write the evolution equations for expectation values and fluctuations:

$$\begin{pmatrix} Q^-_{n+1} \\ P^-_{n+1} \end{pmatrix} = \begin{pmatrix} T_{QQ} & T_{QP} \\ T_{PQ} & T_{PP} \end{pmatrix} \begin{pmatrix} Q^+_n \\ P^+_n \end{pmatrix}, \quad (3.16)$$

$$\begin{pmatrix} \delta\mathbf{Q}^-_{n+1} \\ \delta\mathbf{P}^-_{n+1} \end{pmatrix} = \begin{pmatrix} T_{QQ} & T_{QP} \\ T_{PQ} & T_{PP} \end{pmatrix} \begin{pmatrix} \delta\mathbf{Q}^+_n \\ \delta\mathbf{P}^+_n \end{pmatrix} + \begin{pmatrix} \mathbf{f}(\tau,\omega_0,\gamma) \\ \mathbf{g}(\tau,\omega_0,\gamma) \end{pmatrix}, \quad (3.17)$$

since both $\mathbf{f}$ and $\mathbf{g}$ have zero expectation value. Hereafter we will use non-bold letters to denote expectation values. In order to find what happens over the kick, we note that $\mathbf{Q}$ is continuous and $\mathbf{P}$ has an increment, so

$$\mathbf{Q}^+_{n+1} = \mathbf{Q}^-_{n+1} = \mathbf{Q}_{n+1}, \quad (3.18)$$

$$\mathbf{P}^+_{n+1} = \mathbf{P}^-_{n+1} - V'(\mathbf{Q}_{n+1}). \quad (3.19)$$

Since the potential term has an operator argument we will perform a second-order Taylor expansion. This is the first truncation we need to carry out in order to close the system of equations. From this we get

$$\mathbf{P}^+_{n+1} = \mathbf{P}^-_{n+1} - V'(Q_{n+1}) - V''(Q_{n+1})\delta\mathbf{Q}_{n+1} - \frac{V'''(Q_{n+1})}{2}(\delta\mathbf{Q}_{n+1})^2. \quad (3.20)$$

The potential and its derivatives can now be evaluated numerically since we have no longer an operator as argument. However in order to have an EVM suitable for numerical work, as in Eq. (3.16), we need to take expectation values of all operators. In order to do this we have to calculate, among others, the map for the fluctuation $(\delta Q_{n+1})^2$ so that we can evaluate the above equation for P^+_{n+1}. We proceed by evaluating $(\delta Q_{n+1})^2$ and made another truncation to second order in δ, so that we get a map which is also second order. In an analogous fashion, we obtain the mappings for the fluctuations $(\delta P^+_{n+1})^2$ and $(\delta P^+_{n+1}\delta Q_{n+1} + \delta Q_{n+1}\,\delta P^+_{n+1})$ and after some rearrangement of terms we have the five expectation value maps for Q and P and for the fluctuations[b]

$$Q_{n+1} = T_{QQ}\,Q_n + T_{QP}\,P^+_n, \quad (3.21)$$

[b]Some details are given in Appendix B in quant-ph/0404001.

$$P^+_{n+1} = T_{PQ}\, Q_n + T_{PP}\, P^+_n - V'(Q_{n+1}) - \frac{V'''(Q_{n+1})}{2}(\delta Q_{n+1})^2 \tag{3.22}$$

$$(\delta Q_{n+1})^2 = T^2_{QQ}\,(\delta Q_n)^2 + T^2_{QP}\,(\delta P^+_n)^2 + T_{QQ}\,T_{QP}\,(\delta Q_n\,\delta P^+_n + \delta P^+_n\,\delta Q_n) + f \cdot f, \tag{3.23}$$

$$(\delta P^+_{n+1})^2 = R^2_{PQ}\,(\delta Q_n)^2 + R^2_{PP}\,(\delta P^+_n)^2 + R_{PQ}\,R_{PP}\,(\delta Q_n\,\delta P^+_n + \delta P^+_n\,\delta Q_n) + h_{n+1} \cdot h_{n+1}, \tag{3.24}$$

$$\delta P^+_{n+1}\,\delta Q_{n+1} + \delta Q_{n+1}\,\delta P^+_{n+1} = 2R_{PQ}\,T_{QQ}\,(\delta Q_n)^2 + 2T_{QP}\,R_{PP}\,(\delta P^+_n)^2 + (R_{PQ}\,T_{QP} + R_{PP}\,T_{QQ})(\delta Q_n\,\delta P^+_n + \delta P^+_n\,\delta Q_n) + (h_{n+1} \cdot f + f \cdot h_{n+1}). \tag{3.25}$$

Here the following definitions have been made:

$$h_n \cdot f + f \cdot h_n = \langle \mathbf{h}_n \cdot \mathbf{f} + \mathbf{f} \cdot \mathbf{h}_n \rangle, \tag{3.26}$$

$$\mathbf{h}_n = \mathbf{g} - V''(Q_n)\mathbf{f}, \tag{3.27}$$

$$R_{PQ} = T_{PQ} - V''(Q_{n+1})T_{QQ}, \tag{3.28}$$

$$R_{PP} = T_{PP} - V''(Q_{n+1})T_{QP}, \tag{3.29}$$

and cubic and higher order combinations of h_n, f, δP and δQ have been neglected. In principle, a complete description of the quantum map could be given if one could use all moments $\langle P_m Q_m \rangle$. As an extra approximation, a cutoff frequency has to be introduced in order to calculate expressions which depend on Eq. (3.3), where the divergences introduced by the use of the Markovian approximation show up. We will now use this set of equations to investigate the effects of quantum and thermal contributions to the dynamics of the system. The parameters and potential used are the same of the classical map.

4. Results

In this section we present the results obtained using the maps developed in the previous section. We analyze the shifts that occur in the threshold of chaos for the system as function of the temperature $k_{\mathrm{B}}T$ and $\hbar$. We also investigate how the cutoff frequency influences this behavior.

In Fig. 3 a bifurcation diagram for small values of $\hbar$ and $k_{\mathrm{B}}T$ is shown (small compared with the action and energy scales of the problem). There is, as before, some coexistence of attractors. These are included using simulation of the map over many different initial conditions. As expected, large segments of this diagram are almost equal to the classical counterpart (Fig. 1). There are, however, four very important differences: first of all, and quite visible in the figure, there are chaotic regions that appear far below the classical threshold of chaos ($V_0 = 5.69287$). One of them, at $V_0 \approx 4$, is associated to the second bifurcation of the classical diagram.

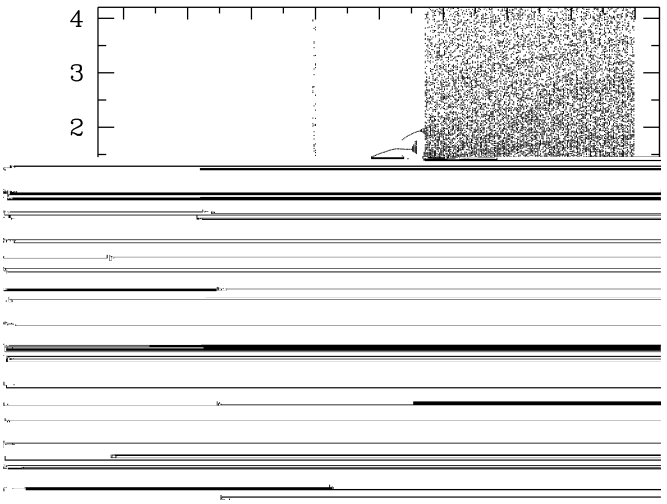

Fig. 3. Bifurcation diagram for the quantized system. We use the same values of γ and τ as in the classical system with a cutoff frequency $\omega_c = 25$. Here 100 random initial conditions are used, and $\hbar = k_{\mathrm{B}}T = 0.0002$. Only the central part of the range in Q is shown for clarity.

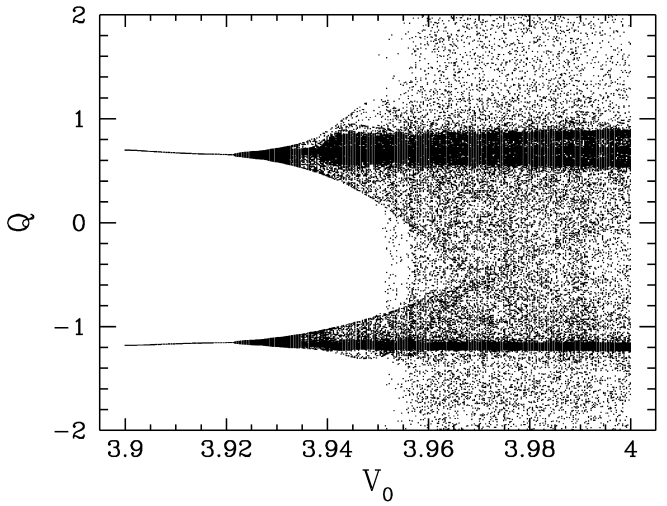

Fig. 4. Magnification of the quantum bifurcation diagram in the second chaotic region, showing the presence of the Hopf bifurcation.

It shows a loss of stability for the quantum system in a parameter sector close to a point where the classical system has a zero Lyapunov exponent. This behavior is shown in Fig. 4, which shows the bifurcation diagram, and Fig. 5, which compares the largest Lyapunov exponent for the quantum and classical maps in this region. Another appears for V_0 around 2.5 and seems to terminate a stable fixed point branch. A similar one appears for $V_0 \approx 5.55$.

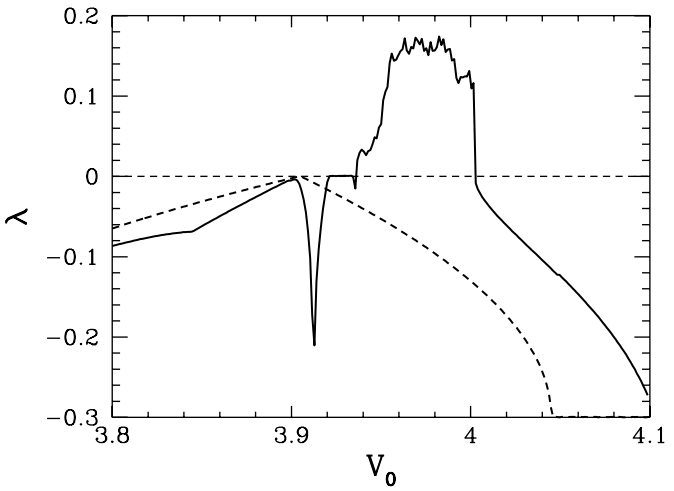

Fig. 5. Comparison of the largest Lyapunov exponents as function of V_0. The dotted line corresponds to the classical case, which undergoes a period doubling bifurcation. In the quantum case (solid line) this is replaced by a Hopf bifurcation followed by a chaotic strip.

Second, and also apparent in Figs. 4 and 5, is the appearance of a Hopf bifurcation just before the chaotic threshold for the quantum map. These transitions are not allowed for the classical system, since it is dissipative and two-dimensional. Here, however, they are preferred over the standard period doubling cascade. We have verified the appearance of simple non-chaotic cycle attractors, typical of Hopf bifurcations, for this transition. It should be noticed that Hopf bifurcations are also present for all other transitions from periodicity to chaos in this map, of which four are visible in Fig. 3 ($V_0 \approx 2.5$, $V_0 \approx 4$, $V_0 \approx 5.55$ and $V_0 \approx 5.7$).

The third main difference between the two bifurcation diagrams is given by the fact that, although the system is still dissipative, there seems to be no clear bound for its variables. Here we are showing Q only for a finite interval, but the numerical simulations generate values of Q as high as several thousands. This peculiarity affects some chaotic regions but not all of them.

Finally, there is no evidence of periodic windows or band mergings inside the chaotic region. There seems to be no topological changes in the chaotic attractor once the last threshold is crossed. Also, a great loss of detail can be clearly inferred from the bifurcation diagram. This is of course even more evident in the attractors themselves, as seen in the example given in Fig. 6. This attractor (at least its projection on the $Q - P$ plane) still resembles the typical attractor for the classical map. Here we are also cropping the figure.

Most of these differences are probably associated with the increase in dimensionality of the map, resulting from the use of the EVM. As mentioned, a Hopf bifurcation would not be possible in the classical system. The behavior of the quantum map, for higher values of $\hbar$ and/or $k_{\mathrm{B}}T$, is similar to the one already described, except for an expected growth of the chaotic strips.

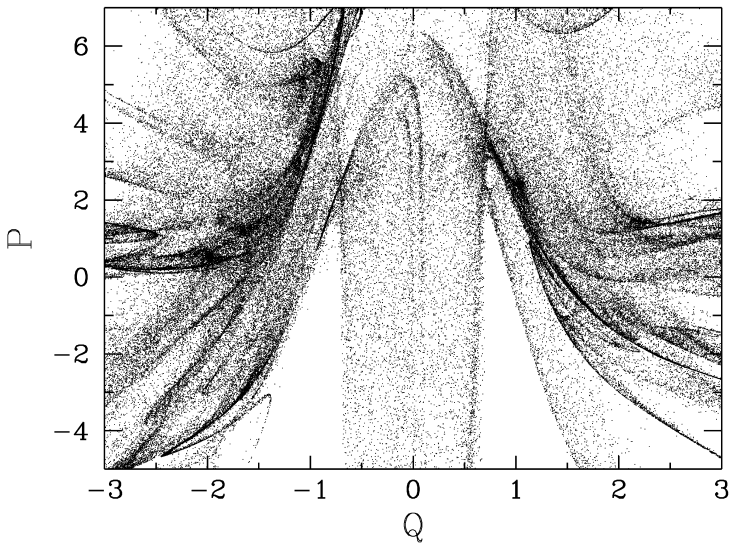

Fig. 6. Attractor for the quantum system using the same parameters as in Fig. 3, and a value of V_0 of 8. Only the central part of the ranges in both P and Q are shown for clarity.

It is also worth mentioning that the attractor (at least its projection on the $Q-P$ plane) still resembles the typical attractor for the classical map (see Fig. 6). It, of course, becomes diffused in the plane, since it is just a projection. Notice that we are strongly cropping this figure, since values of P and Q spread up to the thousandths.

The changes we have mentioned up to now signal qualitative differences between classical and quantum maps. Besides these, we have also studied the evolution of bifurcation points and chaotic thresholds due to changes in $\hbar$ and $k_{\mathrm{B}}T$, assuming always $\hbar \neq 0$, $k_{\mathrm{B}}T \neq 0$. We have obtained the bifurcation point for the last Hopf transition and the last chaotic threshold for different values of $k_{\mathrm{B}}T$ and $\hbar$. In all cases it is found that both points are shifted towards lower values of V_0 with increase of either $k_{\mathrm{B}}T$ or $\hbar$, agreeing with previous results [21, 23], which deduce this behavior from the reduction of quantization and temperature effects to an effective noise. This shift seems to have quadratic scaling in both parameters, in difference with the non-integer exponent change given in [21, 23]. This is not surprising taking into account the strong truncation in the power series we have performed.

The temperature effects can be seen in Fig. 7, where we plot the value of the potential parameter V_0 for which the systems enters the chaotic regime, as function of the temperature $k_{\mathrm{B}}T$. The different curves correspond to fixed values of $\hbar$. The solid line set of curves correspond to the beginning of the Hopf bifurcation where $\lambda = 0$, and the dashed ones are for the beginning of fully developed chaos. Note that even when these curves are not as smooth as the first ones, the general tendency is maintained for all of them. It can be seen how the value of V_0 decreases as

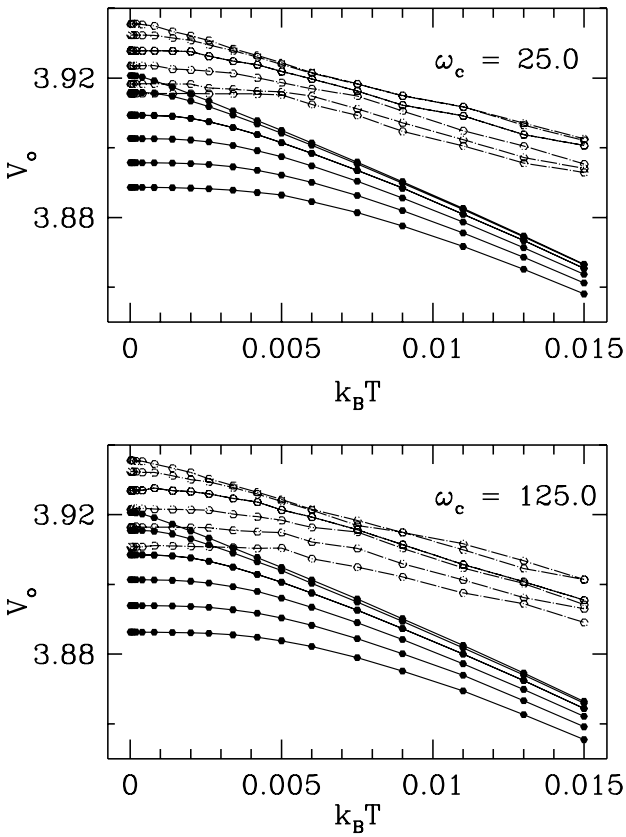

Fig. 7. Plot showing the shift of the chaotic thresholds (dotted line) and the Hopf bifurcation (solid line), with respect to $k_{\mathrm{B}}T$, for two values of the cutoff frequency. Each curve within any of the four bundles corresponds to a different value of $\hbar$. Starting from the upper curve the values of $\hbar$ are 0.0005, 0.002, 0.004, 0.006, 0.008 and 0.01.

$k_{\mathrm{B}}T$ is raised, that is, keeping everything else constant, the greater the temperature, the earlier chaos appears in the system. The cutoff frequency has some effect on the curves, but the general behavior is the same independently of the value of ω_c. The influence of the cutoff frequency is more clearly seen in Fig. 8, which shows the same two transitions, for fixed $k_{\mathrm{B}}T$ and variable $\hbar$, and in Fig. 9 where it is clear that an increase in the cutoff has a similar effect as augmenting the $\hbar$ or the temperature, i.e. it shifts the thresholds for chaos towards lower values of V_0. The scaling of the threshold and bifurcation values with $k_{\mathrm{B}}T$ is quadratic as mentioned before. This can be seen in Fig. 10. This is probably due to the truncation to second order of the whole EVM.

A very similar behavior is obtained when we change the value of $\hbar$. In Fig. 11, the evolution of bifurcation and threshold points is shown for several fixed values of $k_{\mathrm{B}}T$. The tendency as before is to have an early onset of chaos for larger values of $\hbar$. However, a peculiar phenomenon appears here: for small values of the cutoff

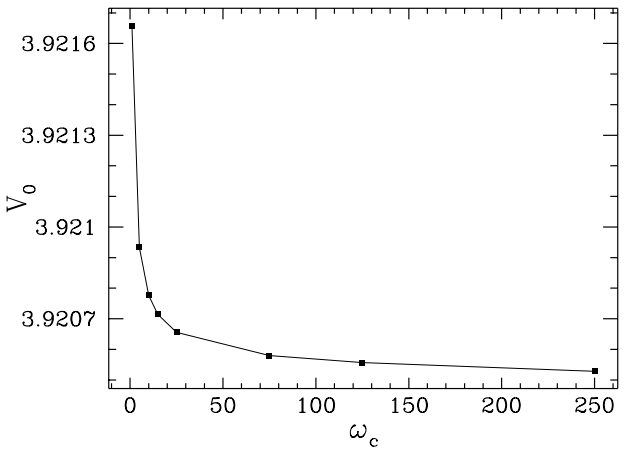

Fig. 8. Effect of the cutoff frequency on the chaotic threshold near $V_0 = 3.92$. Values for $k_{\rm B}T$ and $\hbar$ are fixed at 0.0001 and 0.0005, respectively.

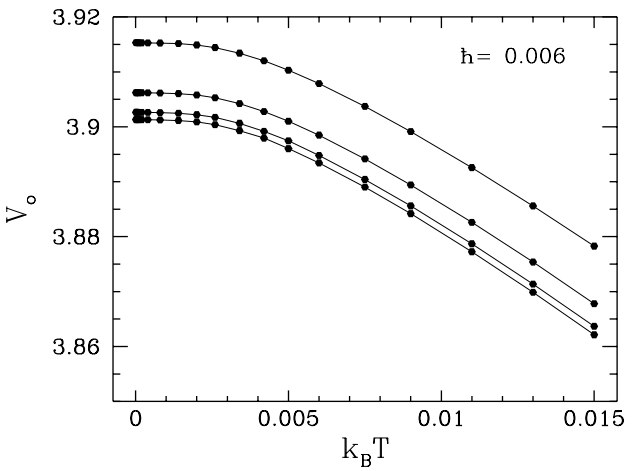

Fig. 9. Beginning of the Hopf transition as a function of $k_{\rm B}T$ for $\hbar = 0.006$ with different values for the cutoff frequency, $\omega_c = 1, 5, 25$ and 125, with ω_c augmenting downwards.

parameter, this tendency is reversed, and the system gets stabilized when $\hbar$ begins to grow, see Fig. 12. This anomalous behavior does not show up when we change $k_{\rm B}T$.

5. Conclusions and Final Comments

The kicked harmonic oscillator with dissipation has been quantized by means of the quantum Langevin equation formalism, truncating the moment expansion up to second order. We obtained the evolution maps for the expectation values Q and P and the second order fluctuations $(\delta Q)^2$, $(\delta P)^2$ and $\delta Q\,\delta P + \delta P\,\delta Q$. The most important result we find is that chaotic behavior appears in a region of parameter

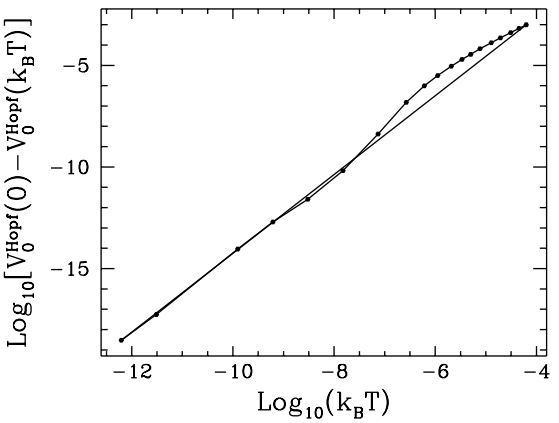

Fig. 10. Logarithmic plot of the beginning of the Hopf transition as function of k_BT. The thin line has slope 2.

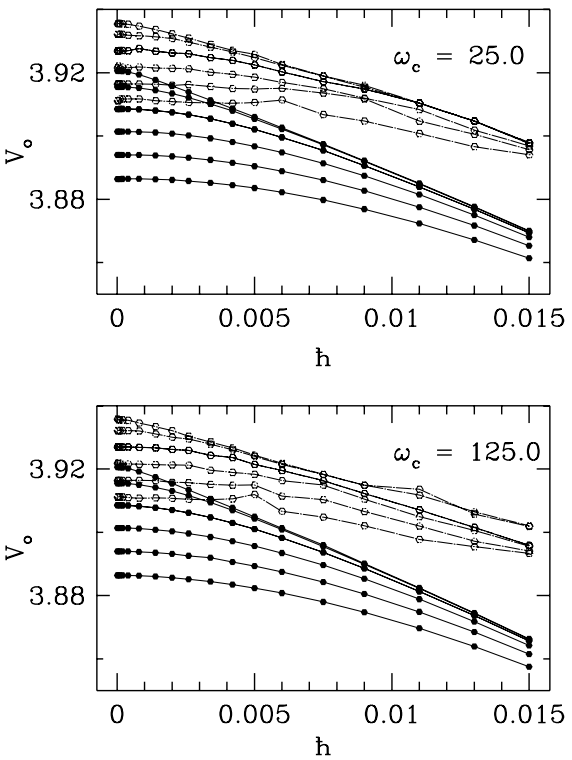

Fig. 11. Plot showing the shift of the chaotic thresholds (dotted line) and the Hopf bifurcation (solid line), with respect to $\hbar$, for two values of the cutoff frequency. Each curve within any of the four bundles corresponds to a different value of k_BT. Starting from the upper curve the values of k_BT are 0.0005, 0.002, 0.004, 0.006, 0.008 and 0.01.

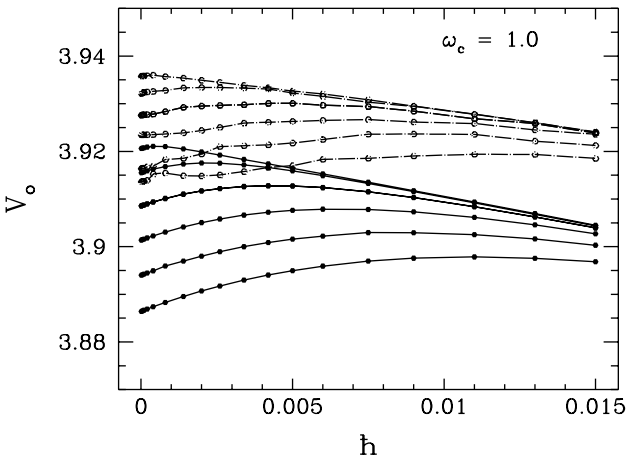

Fig. 12. Anomalous behavior of a chaotic threshold (upper bundle) and Hopf transition (lower bundle) for a low value of the cutoff frequency, as function of $\hbar$. Starting from the upper curve the values of k_BT are 0.0005, 0.002, 0.004, 0.006, 0.008 and 0.01.

space far below the classical threshold for chaos. This agrees with the result reported by Liu and Schieve [26], who also found chaotic behavior in a system whose classical version is periodic. We also find that the change in dimensionality in the map changes the type of bifurcations in the dynamics, as shown by the appearance of Hopf bifurcations on the quantized system. It should be noticed that this is not an artifact of the EVM, since any representation of a quantum system via c-numbers (wave functions in configuration space, elements of the density matrix in any given base, etc.) is infinite dimensional. Therefore, the reduction of a quantum dissipative system to the corresponding classical system plus some noise ignores the possible effects of this change in dimensionality.

Once we are in a finite k_BT and $\hbar$ domain, a continuous displacement of chaotic thresholds and bifurcation points towards lower values of V_0 is observed, as k_BT and $\hbar$ are increased. This agrees with most of the results obtained up to now in this field, and goes to confirm the rule that states that *quantization of Hamiltonian systems eliminates chaos, but dissipative systems become more chaotic when they are quantized*. This is due to the loss of coherence brought in by the dissipative environment. By now, there are some experimental confirmations of this rule [28]. Here we should comment that irregularities observed in the curves for the threshold of chaos in Figs. 7 and 11 are due to the uncertainties incurred in the numerical evaluation of the largest Lyapunov exponent for the system.

We are aware, of course, that a second-order expansion is not sufficient to reproduce the behavior of the infinite dimensional EVM. Hoverer, we doubt that the inclusion of higher order corrections will restore periodic behavior to these new chaotic regions, although it is of course expected that some extra phenomenology will appear with the inclusion of these terms.

We have introduced a cutoff frequency ω_c in order to perform some of the integrals. This cutoff frequency is expected to come from the dimensions of the physical system in a real experiment. The existence of a cutoff implies a breakdown on the Markovian condition, but, as long as $\omega_c \gg \Omega$, assuming that the system is Markovian is not a very strong approximation. In our simulations, we find that this is not a very important parameter except when the obviously inconsistent case when it takes very low values.

Acknowledgments

M.R. wants to thank Cinvestav-IPN and the Fondo Yucatán for partial support. G.P. acknowledges support from CONACyT, under grant 40726-F.

References

1. E. J. Heller, M. F. Crommie, C. P. Lutz and D. M. Eigler, *Nature* **369** (1994) 464.
2. M. F. Crommie, C. P. Lutz and D. M. Eigler, *Science* **262** (1993) 218.
3. B. Eckhardt, G. Hose and E. Pollak, *Phys. Rev.* **A39** (1989) 3776.
4. E. Heller, *Phys. Rev. Lett.* **53** (1984) 1515.
5. M. C. Gutzwiller, *J. Math. Phys.* **8** (1967) 1979; **10** (1969) 1004; **11** (1970) 1791; **12** (1971) 343.
6. M. C. Gutzwiller, *Chaos in Classical and Quantum Mechanics* (Springer-Verlag, 1990).
7. B. Eckhardt, Periodic orbit theory, Lecture notes for the *Int. School of Physics "Enrico Fermi" on Quantum Chaos*, Varena, Villa Monastero, 23 July–2 August 1991.
8. T. Brody, J. Flores, J. French, P. Mello, A. Pandey and S. Wong, *Rev. Mod. Phys.* **53** (1981) 385.
9. M. Methta, *Random Matrices* (Academic Press, 1991).
10. M. D. Kostin, *J. Chem. Phys.* **57** (1972) 3589.
11. H. Dekker, *Phys. Rev.* **A16** (1977) 2116.
12. A. M. Kowalski, A. Plastino and A. N. Proto, *Phys. Rev.* **E52** (1995) 165.
13. R. P. Feynman and F. L. Vernon, *Ann. Phys.* **24** (1963) 118.
14. A. O. Caldeira and A. J. Legget, *Physica* **121A** (1983) 587.
15. A. O. Caldeira and A. J. Legget, *Phys. Rev. Lett.* **46** (1981).
16. U. Weiss, *Quantum Dissipative Systems* (World Scientific, 1993).
17. F. Haake, *Quantum Statistics in Optics and Solid State Physics*, Springer Tracts in Modern Physics, Vol. 66, ed. G. Holler (Springer-Verlag, 1973).
18. H. Haken, *Rev. Mod. Phys.* **47** (1975) 67.
19. G. W. Ford, J. T. Lewis and R. F. O'Connell, *Phys. Rev.* **A37** (1988) 4419.
20. G. W. Ford, J. T. Lewis and R. F. O'Connel, *Phys. Lett.* **A128** (1988) 29.
21. R. Graham and T. Tél, *Z. Phys.* **B60** (1985) 127.
22. C. W. Gardiner, *Quantum Noise* (Springer-Verlag, 1991).
23. H. A. Cerdeira, R. Ramaswamy and A. O. Caldeira, ICTP preprint IC/89/394.
24. D. Cohen, *J. Phys. A: Math. Gen.* **27** (1994) 4805.
25. T. Dittrich and R. Graham, *Z. Phys.* **B62** (1986) 515.
26. W. V. Liu and W. C. Schieve, *Phys. Rev. Lett.* **78** (1997) 3278.
27. M. E. Goggin, B. Sundaram and P. W. Milonni, *Phys. Rev.* **A41** (1990) 5705.
28. H. Ammann, R. Gray, I. Shvarchuck and N. Christensen, *Phys. Rev. Lett.* **80** (1998) 4111.